Evidence for the 3D radiative effects of boundary-layer clouds from observations of direct and diffuse surface solar fluxes

Najda Villefranque[1], Robin J. Hogan[2]

[1]LMD-IPSL, Sorbonne University, CNRS, 4 pl Jussieu, Paris, France
[2]ECMWF, Reading, United Kingdom

Key Points:

- Observed direct–diffuse partition of surface solar radiative fluxes is compared to 1D and 3D radiation calculations performed with ecRad
- Only the radiative transfer solver that includes 3D effects (SPARTACUS) is able to reproduce the observations at large solar zenith angles
- Direct–diffuse partition is mostly sensitive to cloud cover, solar zenith angle, liquid water content, cloud size and effective radius

Corresponding author: Najda Villefranque, najda.villefranque@lmd.ipsl.fr

Abstract

Numerical experiments have revealed the importance of horizontal transport of light in the presence of clouds ("3D effects"), with consequences for climate, weather and solar resource availability predictions. Yet, analysis of 3D effects from observations remain sparse because of the difficulty to isolate the effect of horizontal transport in radiation measurements. In this paper, we provide observational evidence for 3D effects based on the direct–diffuse partition of surface solar fluxes. It is compared to outputs from the ecRad radiative transfer scheme run on retrieved cloud profiles. The direct-beam calculation takes careful account of the field-of-view of the pyrheliometer to ensure consistency between observed and modeled direct fluxes. Only the solver that accounts for 3D effects is able to reproduce the observed mean direct–diffuse partition as a function of solar zenith angle and cloud cover, in particular at large solar zenith angles where cloud sides intercept most of the direct beam.

Plain Language Summary

Accurately predicting the amount of solar energy that reaches the surface is of crucial importance for future climate projections and weather forecast, as well as for the solar energy industry. Atmospheric models include radiative transfer schemes, which are numerical models that represent the physical processes involved in the propagation of solar radiation. Understanding and modeling the impact of low-level clouds on solar radiation can be particularly challenging due to their frequent complex geometry. In this study, we provide observational evidence for the "3D radiative effects of clouds", which are mostly due to the fact that cloud sides intercept the direct solar beam when the sun is low in the sky. To achieve this, we compare observations of surface radiation with outputs from numerical models that do and do not include a representation of 3D effects. We find good agreement between observed and modeled radiation on average only if 3D effects are taken into account in the radiative transfer scheme. Cloud 3D radiative effects are entirely missing from current atmospheric models; our results support the argument that they should be included. The radiative transfer scheme we use appears to be a promising candidate for future use in weather and climate models.

1 Introduction

Accurate predictions of the amount of solar radiation that reaches the surface under diverse atmospheric conditions are needed for various sensitive applications such as simulation of climate change, weather forecasts, and design and control of solar energy systems (see e.g. Lopes et al. (2018) and references therein). Boundary-layer clouds in particular have a major impact on solar surface radiation at different scales as they cover a large fraction of the Earth's continents and oceans during most of the time and are optically thick to sunlight (Berg et al., 2011; Burleyson et al., 2015).

Radiative transfer parameterizations that are used in large-scale models to predict the solar radiative effect of clouds neglect 3D effects that are due to horizontal propagation of light. Long-standing efforts have been made to characterize 3D effects and understand the physical processes that drive them (e.g. McKee and Cox (1974); Várnai and Davies (1999)), their dependency on the cloud-field properties (e.g. Hinkelman et al. (2007)) and their potential impacts on microphysics and macrophysics (e.g. Jakub and Mayer (2017)). An important and complementary aspect is the development of 3D parameterizations for both large-scale (e.g. the SPeedy Algorithm for Radiative TrAnsfer through CloUd Sides (SPARTACUS); Hogan and Shonk (2013); Hogan et al. (2016, 2019)) and cloud-resolving models (e.g. the ten-stream model; (Jakub & Mayer, 2015)).

All these studies rely on numerical experiments; evidence of 3D effects in surface observations have remained elusive. Recently, Gristey et al. (2020b) have provided such observational evidence by demonstrating that the bimodality characteristic of the distribution (PDF) of surface solar irradiance observed under cumulus cloud fields is a signature of the 3D radiative effects of clouds. They used high-resolution cloud fields from Large-Eddy Simulations and Monte Carlo models to compare PDFs obtained from 1D and 3D simulations to PDFs obtained from observations, and found that only 3D computations can reproduce the PDF shape. They also show that 3D effects always increase the diffuse flux component at the surface — which they explain by entrapment of light through non-vertical reflections and diffuse radiation escaping from cloud sides — and that they most often decrease the direct flux component, which they explain by interception of direct light by cloud sides. They suggest that taking these effects into account in surface radiation forecasts might be particularly important for the solar energy industry.

While many other arguments can be found in the literature in favor of atmospheric models using 3D radiative transfer (RT) schemes instead of remaining with the 1D paradigm, the resulting cost–benefit balance remains to be weighted for models at different scales. For example, it is unknown how much representing 3D effects in long-term climate simulations might affect cloud properties, either directly through the feedback of surface fluxes and heating rates on atmospheric processes or through the cloud parameter values selected during the tuning process, in which cloud–radiation interactions play an important role (Hourdin et al., 2017). The development of SPARTACUS, a 3D RT parameterization that is fast enough to be used in global simulations (at least for research purposes) is an important element in this landscape. However, its use in climate simulations should be accompanied by a thorough evaluation of its capacity to represent 3D cloud–radiation interactions and a rigorous quantification of related uncertainties. Previous studies have shown reasonably good agreement between SPARTACUS and 3D RT models run of detailed 3D cloud fields output from high-resolution atmospheric models (Hogan et al., 2016, 2019; Villefranque et al., 2021). However, process-based evaluation of the cloud part of a RT scheme using radiation observations remains difficult because the 3D clouds above measured radiative fluxes are often unsufficiently constrained.

In this paper, boundary-layer cloud vertical profiles retrieved from observations at the ARM Graciosa site and processed by the Cloudnet analysis system (Illingworth et al., 2007) are ingested by two versions of the ecRad radiation scheme (Hogan & Bozzo, 2018): one that includes 3D effects (SPARTACUS) and one that does not (Tripleclouds; Shonk and Hogan (2008)). Ratios of direct to total surface solar fluxes (DTRs) obtained from parameterized 1D and 3D computations are compared to DTRs computed from ARM measurements, as a function of cloud cover and solar zenith angle. Sensitivity analysis are performed to assess the relative importance of input data, model parameters and 3D effects in the average accuracy of the DTR predictions.

Through our analysis, we provide:

- observational evidence of 3D radiative effects of clouds in the ratio of direct to total solar surface fluxes (DTR). While Gristey et al. (2020b) based their conclusions on the analysis of a few high-resolution 3D cloud fields, ours are rather based on long-term datasets of horizontally integrated cloud and radiation measurements;
- observation-based statistical validation of the solar component of SPARTACUS in the presence of boundary-layer clouds.

The remainder of the manuscript is organized as follows. Section 2 describes the ARM and Cloudnet data, the ecRad model and the methodology that is used to

analyze the DTRs. Section 3 presents the resulting observed, 1D and 3D DTRs as a function of cloud cover and solar zenith angle, as well as a sensitivity analysis on various model parameters. Finally, some implications of our findings are discussed in Section 4.

2 Method

The radiation observations used in this study consist of hourly averaged direct and total surface downwelling solar fluxes measured at the Graciosa island in the Azores archipelago. A first dataset, refered to as D1, consists of 19 months of hourly data from 5th June 2009 to 31st December 2010 and a second dataset (D2) consists of 26 months of hourly data from 17th July 2015 to 21st September 2017. Observations of downwelling solar radiation at the surface were taken from the Atmospheric Radiation Measurement (ARM) data (Atmospheric Radiation Measurement (ARM) user facility, 2009a, 2013a). The first dataset D1 corresponds to the data acquired by the ARM Mobile Facility deployed during the Clouds, Aerosol and Precipitation in the Marine Boundary Layer (CAP-MBL) campaign (Wood et al., 2015), and D2 corresponds to measurements acquired by the permanent observatory installed in 2013. Hourly-averaged broadband direct and total solar downwelling fluxes measured at the surface are used to compute the direct-to-total flux ratio (DTR). The direct flux is measured by a pyrheliometer characterized by a field-of-view of 5.7°. The total hemispheric flux is measured by a pyranometer. Only low clouds are considered in this study: cloud profiles where the maximum cloud fraction above 2500 meters is larger than 5% are excluded.

Rather than studying individual cases, DTRs are analyzed statistically, by averaging in bins of cloud cover and solar zenith angle (SZA). Both direct and total fluxes decrease when either cloud cover or SZA increases, but they do not decrease at the same rate, hence DTRs are also sensitive to cloud cover and SZA. For each hour, the observed DTR is associated with the corresponding hourly averaged SZA value and with the hourly averaged cloud cover value provided by the ARM Total Sky Imager (Atmospheric Radiation Measurement (ARM) user facility, 2009b, 2013b). The DTR is then attributed to one of five cloud-cover sub-intervals ([0.1–0.3], [0.3–0.5], [0.5–0.7], [0.7–0.9], [0.9–1]), and to one of nine SZA sub-intervals (obtained from applying the inverse cosine function to a regular division of the [0.05–1] interval). The DTRs are averaged within each 2D bin and the associated 95% confidence interval width is computed in each bin as 1.96 times the standard deviation of the data divided by the square root of the number of independent samples in the bin. Samples are independent if they are separated by at least six hours of time, following Hogan et al. (2009) who found that this is the approximate e-folding time for cloud occurrence autocorrelation in cloud radar data.

Observed boundary-layer clouds coincident with observed radiation are then used as inputs to ecRad to compute 1D and 3D DTRs. Cloud fraction, mean liquid water content (LWC) and horizontal standard deviation of LWC (FSD) profiles are taken from the Cloudnet analysis system (Illingworth et al., 2007), which uses the same ARM measurements and provides retrievals averaged onto the grid of the ECMWF Integrated Forecasting System (IFS). Only the D1 dataset is used as the liquid water path available in D2 Cloudnet products appeared to be unreliable at the time of the analysis. Cloud fraction profiles at the resolution of the model are computed from high resolution (60 meters, 30 seconds) target categorization profiles based on lidar backscatter, radar reflectivity and Doppler velocity. The cloud cover is also diagnosed from the high-resolution categorization profiles, as the fraction of profiles containing clouds in each period of one hour. LWC profiles are computed following the scaled adiabatic method: the adiabatic liquid water content is calculated from temperature in each separate cloud layer from cloud base derived from the Micro Pulse Lidar to

cloud top derived from the profiling radar. Then the LWC values are scaled to match the liquid water path (LWP) as inferred from microwave radiometer measurements. Data including precipitation at the surface are excluded because of unreliable LWP measurements. Profiles of mean LWC and standard deviation of non-zero LWC are then computed at each hour. Figure 1(a) and (b) present 72-hours-long timeseries of LWC and cloud fraction profiles for illustration. In order to exclude profiles where high clouds are present, hours when the maximum observed cloud fraction above 2500 m is greater than 5% are filtered out. Temperature, pressure, water vapour content and ozone concentration are taken from the IFS high-resolution forecast at the gridpoint closest to Graciosa Island, and aerosol and trace gas concentrations are taken from the same climatology as the IFS. Two sensitivity tests are performed to assess the uncertainty related to the Cloudnet retrievals, one with FSD=0.75 (Shonk et al., 2010) and one using LWC profiles scaled by 1.5.

Other cloud parameters that could not be directly derived from local observations are set according to the literature, yielding a reference configuration. Sensitivity tests are performed for each parameter separately (in each sensitivty test, all other parameters are kept to their reference values). The effective radius of liquid droplets r_e is set to 8.2 μm in the reference configuration, according to aircraft data collected in maritime clouds during the ASTEX campaign (Yum & Hudson, 2002). A sensitivity test is performed using $r_e = 12.4$ μm, which is the average value reported by Dong et al. (2014), based on retrievals from LWP and solar radiation observations in Graciosa single-layered clouds during the CAP-MBL campaign. The overlap decorrelation length z_0 that appears in the exponential-random overlap scheme used in Tripleclouds and SPARTACUS is set to 2000 m in the reference configuration and 1000 m in the sensitivity test (Barker, 2008; Hogan & Illingworth, 2000). The cloud-edge length that is needed in SPARTACUS is parameterized as a function of cloud fraction and an effective cloud spacing parameter C_x, set to 2000 m in the reference configuration and 1000 m in the sensitivity test, following Fielding et al. (2020). The surface albedo α is set to 15% in the reference configuration to represent the radiative effect of the surface in a 2-km radius circle around the observatory. It is a weighted average of the sea value (around 6%) and the locally observed value, around 20% (on average, computed from the ratio of upward to downward flux at the surface, not shown), in which slightly more land is accounted for. A sensitivity test is performed with $\alpha = 7.5\%$.

Modeled DTRs are computed using the ecRad radiation scheme (Hogan & Bozzo, 2018). Radiative transfer is solved using variants of a two-stream model. In the 1D solver Tripleclouds (Shonk & Hogan, 2008), the two-stream equations are modified to represent cloud geometry effects due to layers being only partially occupied by clouds, the degree of vertical overlap of the cloudy regions in different layers, and in-cloud liquid water content variability. In the 3D solver SPARTACUS (Schäfer et al., 2016; Hogan et al., 2016, 2019), terms are added to the Tripleclouds scheme to represent the effects of horizontal transport of light: photons escaping through cloud sides, entrapment of light due to non-vertical reflections, and interception of direct light by cloud sides when the sun is not at zenith. For a given cloud fraction, the intensity of these effects increases with the number of clouds: more clouds means a larger area of cloud sides through which radiation can flow. The output DTRs are binned according to the cloud cover value diagnosed by ecRad, which depends on the input Cloudnet cloud fraction profile and on the vertical overlap assumptions. Note that the cloud cover estimates used to bin the modeled and observed DTRs are inconsistent with each other but consistent with the nature of the DTR: observed DTRs were computed from radiation measurements that have "seen" the whole sky thus they are associated with hemispheric cloud covers diagnosed by the TSI, while modeled DTRs were computed from simulated radiation that has only "seen" vertical profiles thus they are associated with cloud covers derived from these profiles.

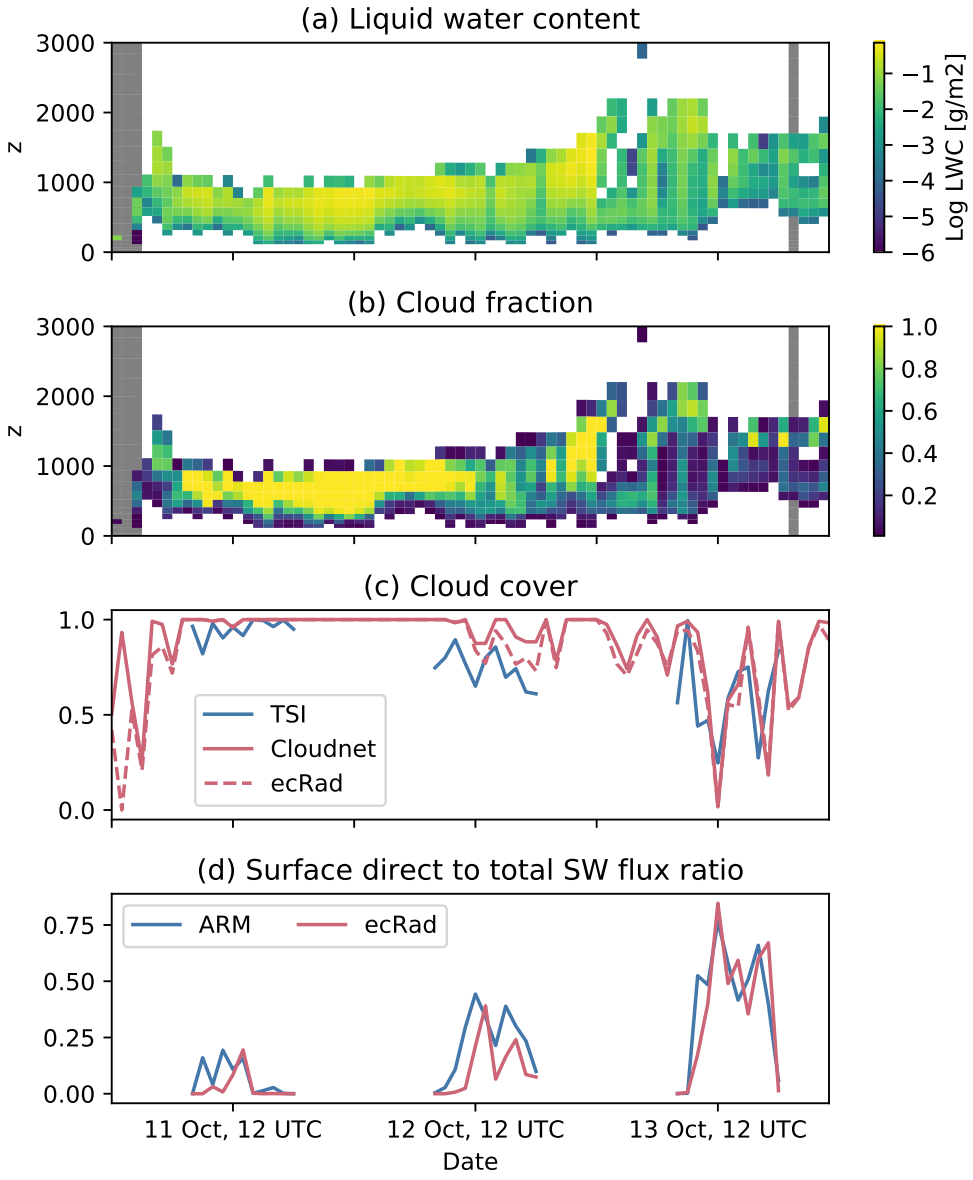

Figure 1. Timeseries of (a) Cloudnet liquid water content, (b) Cloudnet cloud fraction profiles, (c) cloud cover diagnosed by the Total Sky Imager (TSI), from Cloudnet categorization profiles and by ecRad using the Cloudnet cloud fraction profiles along with vertical overlap assumptions, (d) DTRs in ARM observations and from ecRad using the SPARTACUS solver run on the Cloudnet cloud profiles. Gray shadings in (a) and (b) correspond to profiles where the maximum cloud fraction above 2500 m is greater than 5%, which were excluded from the analysis.

To be able to compare observed and modeled DTRs, the definition of direct flux should be the same in the two worlds. The pyrheliometer measures radiation incident into a normal plane to the sun direction and into a small solid angle around the sun direction. However, most radiation schemes, including ecRad, rely on the delta-Eddington approximation of Joseph et al. (1976), which treats a fraction f of the forward-scattered radiation as if it had not been scattered at all, thereby increasing the radiation treated as "direct" to include more than purely unscattered radiation from the sun. In this approximation, optical properties are scaled to replace thick clouds characterized by strongly asymetric phase functions that scatter most of the energy into a small forward solid angle, by optically thinner clouds with phase functions closer to isotropic. The resulting reduction of the attenuation of the direct beam is compensated by an increase of backward scattering. While this increases the accuracy of total flux estimates, the "direct" flux can no longer be compared directly to pyrheliometer measurements. To ensure consistency between the definition of the modeled direct flux and the flux seen by a pyrheliometer, Räisänen and Lindfors (2019) derived a parameterization for the delta-scaling factor that depends on the FOV angle of the instrument and on the effective radius of the liquid droplets or ice crystal size distribution. A slightly simpler approach was taken here, whereby the delta-Eddington factor is scaled by a further value β, that is then assumed constant in ecRad calculations:

$$f_{corr} \;=\; \beta \;\times\; f_{Edd} \;\approx\; f_p$$

where $f_{Edd} = g^2$ is the delta-Eddington scaling factor (where the asymmetry factor, g, is the average of the cosine of the scattering angle) and f_p is the fraction of energy that is scattered into a 2.85° forward angle (the half width of the field-of-view of the pyrheliometer). The computation of β uses detailed phase functions computed from the Mie theory, integrated over gamma size distributions parameterized by the effective radius $r_e = 10\mu m$ and various effective variances v_e (the same data underly the cloud optics parameterization SOCRATES used in ecRad; Manners et al. (2017)). This is shown in Figure 2. β is in fact a decreasing function of the wavelength and ranges from 0.61 to 0.42 between 400 and 1600 nm (not shown). In the following, it is set uniformly to 0.6 for the reference configuration, and sensitivity tests are performed with $\beta = 1$ and $\beta = 0.5$. For each configuration, ecRad is called twice on each column: once with $f = f_{Edd}$ to produce appropriate estimations of the total flux and once with $f = f_{corr}$ to produce appropriate estimations of the direct flux.

To measure the quality of a particular ecRad configuration compared to ARM measurements, an error metric is computed for each of the five cloud cover values × nine solar zenith angle sub-intervals as:

$$I_m(c,\theta_0) = \frac{|\mathrm{DTR}_{obs}(c,\theta_0) - \mathrm{DTR}_m(c,\theta_0)|}{\sqrt{\sigma_{obs}(c,\theta_0)^2 + \sigma_m(c,\theta_0)^2}} \tag{1}$$

where m is the model configuration, (c,θ_0) the cloud cover × solar zenith angle sub-interval, $\mathrm{DTR}_{obs}(c,\theta_0)$ is the ARM mean DTR in the (c,θ_0) sub-interval, $\mathrm{DTR}_m(c,\theta_0)$ is the mean DTR predicted by ecRad configuration m in (c,θ_0) and $\sigma_{obs}(c,\theta_0)$ (respectively $\sigma_m(c,\theta_0)$) is the standard deviation associated with $\mathrm{DTR}_{obs}(c,\theta_0)$ (respectively, $\mathrm{DTR}_m(c,\theta_0)$). The normalization is a way to account for the uncertainties due to internal variability and limited sampling within the sub-intervals. If $I_m(c,\theta_0) < 1$, it means the model error is dominated by the statistical uncertainty associated with the averaging method. Otherwise, the model–observation distance becomes significant. To summarize the error over all the (c,θ_0) bins, two metrics are used:

$$I_{m,\max} = \max_{(c,\theta_0)} \{I_m(c,\theta_0)\} \quad \text{and} \quad I_{m,L2} = \sqrt{\sum_{(c,\theta_0)} I_m(c,\theta_0)^2} \tag{2}$$

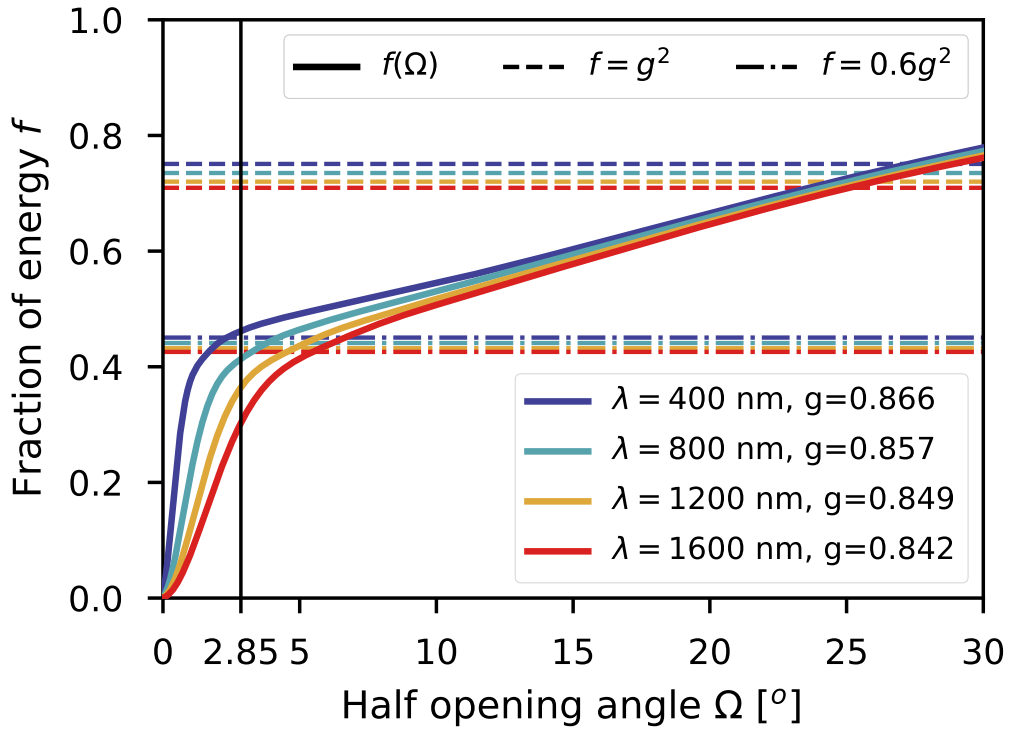

Figure 2. Fraction f of radiation scattered by liquid droplets (y-axis) in a forward half-angle of aperture Ω, computed from Mie phase functions integrated over gamma size distributions with effective radius $r_e = 10$ μm and varying effective variances (see text) for four wavelengths over the visible and near-infrared spectrum. Solid lines give f as a function of Ω; dashed lines correspond to values of f that are used in the δ-Eddington approximation ($f = f_{Edd} = g^2$ where g is the phase function asymmetry parameter); point-dashed lines correspond to $f = f_{corr} = \beta \times f_{Edd}$ with $\beta = 0.6$. The vertical black line corresponds to the half angle of the field-of-view of the ARM pyrheliometer.

3 Results

The observed and modeled direct-to-total fluxes ratios (DTRs) are shown in Figure 3 as a function of cloud cover and SZA. Observational data cover the 2009-2010 (D1) and 2015-2017 (D2) time periods while modeled DTRs only include data from D1. Both modeled and observed data show that the average DTR decreases with increasing cloud cover because the direct flux decreases more rapidly than the total flux. Both modeled and observed data show that average DTRs also decrease with increasing SZA. The mechanism for this in the 1D case represented by Tripleclouds is the increased path length through the atmosphere leading to more rapid attenuation of the direct beam when the sun is lower in the sky. The speed of decrease is highly sensitive to the representation of 3D effects: neglecting these effects leads to inaccurate dependency of the DTR to the SZA, while taking them into account leads to good agreement between modeled and observed DTRs. Indeed, both direct and diffuse fluxes are modified by 3D effects: they decrease the direct surface flux by enhancing the interception of the direct beam by cloud sides and they increase the diffuse surface flux by enhancing cloud side reflection and entrapment. Both effects lead to a decrease of DTR when the intensity of 3D effects increases, i.e. when the sun approaches the horizon. Representing 3D effects is crucial to reproduce the rate of decrease of DTRs with solar angle. Discrepancies remain between modeled and observed DTRs for small SZAs at large cloud covers. Since this behaviour was not evidenced in previous studies comparing SPARTACUS to 3D RT models when cloud fields were perfectly known (e.g. Hogan et al. (2019)), it is probable that uncertain cloud and radiation parameters are first responsible for these discrepancies rather than the misrepresentation of an important process in the SPARTACUS scheme itself, although this remains to be demonstrated. However, the disagreement in the [0.9–1] cloud cover bin demonstrates that this discrepancy is not likely to be due to 3D effects.

Sensitivity tests were performed to analyze the dependency of DTRs to various cloud characteristics, quantify the relative importance of 3D effects on the DTR estimates and probe the increase in SPARTACUS DTR estimates accuracy that could be gained by finer tuning of free parameters. For each configuration, the two errors metrics $I_{m,\max}$ and $I_{m,L2}$ are shown in Figure 4. Comparing $I_{m,\max}$ and $I_{m,L2}$ for 1D and 3D ecRad configurations shows that 3D effects are a key ingredient to significantly reduce the distance between the observed and modeled DTRs. The other parameters that most affect the DTRs and might explain the remaining discrepancies between observations and model outputs seen in Figure 3 are: the liquid water content (LWC) and its fractional standard deviation (FSD), which might be biased in the retrievals; the effective radius r_e which was set to a constant value instead of a function of LWC; the cloud spacing parameter C_x that controls the intensity of 3D effects; and the β factor that was applied to correct delta-scaling, which drastically modifies the estimate of direct flux. Surface albedo and overlap parameters have small impact: doubling the surface albedo only slightly increases the total downward flux at the surface, while changing the overlap parameter both changes radiation and cloud cover and hence preserves the average DTR computed over a given cloud cover sub-interval. These results agree with previous studies, for instance similar parameters were found to explain the PDF of surface solar irradiance under 3D cumulus clouds using machine learning in Gristey et al. (2020a). Note however that since the extent to which the different parameters were perturbed is not uniform, their relative importance was not thoroughly quantified here.

4 Conclusions

In this paper, observations of the partition of solar surface fluxes into direct and diffuse components have been analyzed. It was demonstrated that the dependency of the DTR to solar zenith angle can only be reproduced by a radiative transfer scheme

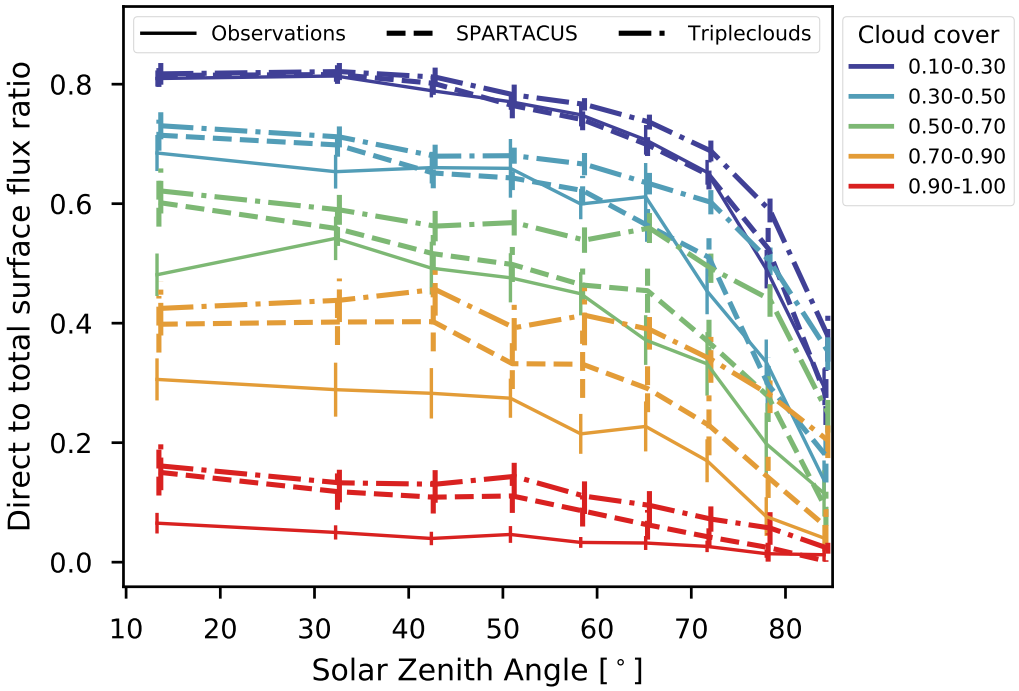

Figure 3. Average direct-to-total ratio of solar surface fluxes as a function of solar zenith angle. The solar zenith angle was discretized into nine sub-intervals. Colors correspond to five different cloud cover intervals. Solid lines correspond to observations, dashed lines correspond to ecRad outputs using the SPARTACUS 3D solver, point-dashed lines correspond to ecRad outputs using the Tripleclouds 1D solver. Error bars indicate the 95% confidence interval around the average value.

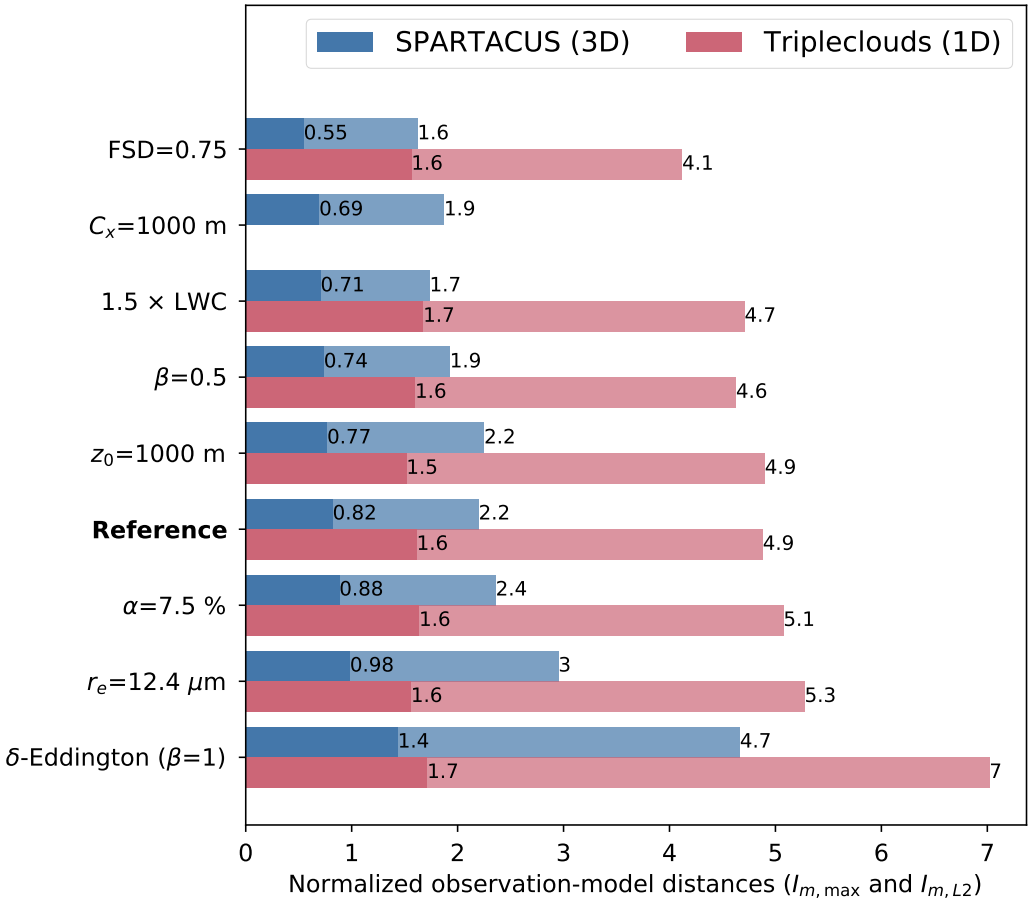

Figure 4. Maximum and L2 errors (see Equations 1 and 2) associated with different configurations of ecRad. The label on the y-axis indicates the change in configuration with respect to the "**Reference**" configuration, which is as follows: the liquid water content profile (LWC) and the fractional standard deviation of in-cloud liquid water (FSD) are taken from the Cloudnet retrievals, the delta-scaling correction factor β=0.6, the cloud spacing parameter $C_x = 2000$ m, the surface albedo $\alpha = 15\%$, the overlap decorrelation length $z_0 = 2000$ m, the effective radius $r_e = 7$ μm. Each bar gives the maximum (dark shading) and L2-norm (light shading) of errors computed over the five cloud cover values × nine solar zenith angles sub-intervals (see text), with associated numbers given at the right side of each bar. Blue bars are associated with the SPARTACUS solver that accounts for 3D effects and red bars are associated with the Tripleclouds solver that neglects 3D effects. The C_x parameter is not used in Tripleclouds hence the missing red bar.

that represents 3D effects. This is observational evidence for the 3D radiative effects of boundary layer clouds. The SPARTACUS solver that was used to simulate sub-grid 3D propagation of radiation produces accurate estimates of the DTRs on average. It implies that SPARTACUS is treating 3D solar effects well, particularly the interception of the direct beam by cloud sides, giving confidence to its potential future use in weather and climate models.

The analysis was based on statistical comparisons rather than direct comparison of time series. One of the main reasons is that cloud profiles provided as inputs to ecRad are only a sub-sample of the 3D atmosphere that was "seen" during the same hour by the radiation instruments. If the structure of the cloud field is not random then there is no reason for the vertical profiles to be representative of the whole cloud field and the associated radiation cannot be compared. Our statistical approach has other limitations: uncertainties due for instance to the cloud cover estimate used to bin the measured DTRs or to the limited amount of data. Further work should aim at reducing these uncertainties for instance by adding newly acquired measurements.

The sensitivity of the DTRs to input data and parameters was also investigated. Uncertainties in the retrieval of the profiles of cloud properties (such as the mean LWC and its subgrid variability) or unsufficiently constrained parameters (such as effective radius or cloud spacing) might explain discrepancies between SPARTACUS and the observations. This could be further investigated by an extensive sensitivity analysis in which SPARTACUS parameter space would be thoroughly explored, for instance using the same approach as in Villefranque et al. (2020).

Another point is that direct flux output from radiation models that use the delta-Eddington approximation should not be compared directly to observations. Depending on the application, predictions of the direct surface flux might need to be corrected to ensure consistency between the size of the direct beam in the model and the one that is relevant to the application. This issue was also raised by Sun et al. (2016) and Räisänen and Lindfors (2019). The latter proposed a sophisticated parameterization to scale the cloud optical properties as a function of the instrument field-of-view. Their parameterization is an alternative to the delta-Eddington scaling factor of Joseph et al. (1976). Here, we propose another solution that consists in scaling the delta-Eddington factor by a correction factor β, which was only appropriate because only liquid boundary-layer clouds with uniform effective radii were considered in this study.

This study provides observational support for the argument that 3D effects should be represented in large-scale models. Models need to provide accurate estimates of surface radiative fluxes to users, in particular to the actors of the solar energy industry who need this information to design systems and optimize their productivity — a major challenge in the context of the large-scale energy transition that is urgently needed. The statistical evidence of 3D radiative effects of clouds we found in surface observations also motivates the need to investigate their impact on climate sensitivity and global climate change.

Acknowledgments

N. V. was funded by the ERASMUS+ program and by l'École des Docteurs de Toulouse for her two-month visit at the ECMWF during her PhD studies. We thank Maike Ahlgrimm, Alessio Bozo, Mark Fielding and Ewan O'Connor for interesting discussions. We are grateful for the helpful work accomplished by two anonymous reviewers. N. V. thanks Françoise Guichard for her everlasting support and inspiring enthusiasm for observational datasets. The data used for this study is available under DOI:10.14768/2bfb2db9-f438-4937-a1fa-bac45b4db6f7.

References

Atmospheric Radiation Measurement (ARM) user facility. (2009a). *Data Quality Assessment for ARM Radiation Data (QCRAD1LONG). 2009-04-16 to 2011-01-06, ARM Mobile Facility (GRW) Graciosa Island, Azores, Portugal; AMF1 (M1).* Data set accessed 2019-07-01 at http://dx.doi.org/10.5439/1227214. (Compiled by D. Zhang and C. Long. ARM Data Center.)

Atmospheric Radiation Measurement (ARM) user facility. (2009b). *Total Sky Imager (TSISKYCOVER). 2009-04-14 to 2011-01-05, ARM Mobile Facility (GRW) Graciosa Island, Azores, Portugal; AMF1 (M1).* Data set accessed 2019-07-01 at http://dx.doi.org/10.5439/1025308. (Compiled by V. Morris and D. Flynn. ARM Data Center.)

Atmospheric Radiation Measurement (ARM) user facility. (2013a). *Data Quality Assessment for ARM Radiation Data (QCRAD1LONG) 2013-10-03 to 2019-10-17, Eastern North Atlantic (ENA) Graciosa Island, Azores, Portugal (C1).* Data set accessed 2019-07-01 at http://dx.doi.org/10.5439/1227214. (Compiled by L. Riihimaki, Y. Shi, D. Zhang and C. Long. ARM Data Center.)

Atmospheric Radiation Measurement (ARM) user facility. (2013b). *Total Sky Imager (TSISKYCOVER). 2013-10-01 to 2021-03-10, Eastern North Atlantic (ENA) Graciosa Island, Azores, Portugal (C1).* Data set accessed 2019-07-01 at http://dx.doi.org/10.5439/1025308. (Compiled by V. Morris and D. Flynn. ARM Data Center.)

Barker, H. W. (2008). Overlap of fractional cloud for radiation calculations in gcms: A global analysis using cloudsat and calipso data. *Journal of Geophysical Research: Atmospheres*, *113*(D8). doi: 10.1029/2007JD009677

Berg, L. K., Kassianov, E. I., Long, C. N., & Mills, D. L. (2011, January). Surface summertime radiative forcing by shallow cumuli at the Atmospheric Radiation Measurement Southern Great Plains site. *Journal of Geophysical Research-Atmospheres*, *116*, D01202. (WOS:000286058200002) doi: 10.1029/2010JD014593

Burleyson, C. D., Long, C. N., & Comstock, J. M. (2015). Quantifying Diurnal Cloud Radiative Effects by Cloud Type in the Tropical Western Pacific. *Journal of Applied Meteorology and Climatology*, *54*(6), 1297 - 1312. doi: 10.1175/JAMC-D-14-0288.1

Dong, X., Xi, B., Kennedy, A., Minnis, P., & Wood, R. (2014). A 19-Month Record of Marine Aerosol–Cloud–Radiation Properties Derived from DOE ARM Mobile Facility Deployment at the Azores. Part I: Cloud Fraction and Single-Layered MBL Cloud Properties. *Journal of Climate*, *27*(10), 3665 - 3682. doi: 10.1175/JCLI-D-13-00553.1

Fielding, M. D., Schäfer, S. A. K., Hogan, R. J., & Forbes, R. M. (2020). Parametrizing cloud geometry and its application in a subgrid cloud-edge erosion scheme. *Quarterly Journal of the Royal Meteorological Society*, *146*(729), 1651-1667. doi: 10.1002/qj.3758

Gristey, J. J., Feingold, G., Glenn, I. B., Schmidt, K. S., & Chen, H. (2020a). On the relationship between shallow cumulus cloud field properties and surface solar irradiance. *Geophysical Research Letters*, *47*(22), e2020GL090152. doi: https://doi.org/10.1029/2020GL090152

Gristey, J. J., Feingold, G., Glenn, I. B., Schmidt, K. S., & Chen, H. (2020b). Surface solar irradiance in continental shallow cumulus fields: Observations and large-eddy simulation. *Journal of the Atmospheric Sciences*, *77*(3), 1065 - 1080. doi: 10.1175/JAS-D-19-0261.1

Hinkelman, L. M., Evans, K. F., Clothiaux, E. E., Ackerman, T. P., & Stackhouse, P. W. (2007). The effect of cumulus cloud field anisotropy on domain-averaged solar fluxes and atmospheric heating rates. *Journal of the Atmospheric Sciences*, *64*(10), 3499-3520. doi: 10.1175/JAS4032.1

Hogan, R. J., & Bozzo, A. (2018). A flexible and efficient radiation scheme for the

ECMWF model. *Journal of Advances in Modeling Earth Systems*. doi: 10.1029/2018MS001364

Hogan, R. J., Fielding, M. D., Barker, H. W., Villefranque, N., & Schäfer, S. A. K. (2019). Entrapment: An Important Mechanism to Explain the Shortwave 3D Radiative Effect of Clouds. *Journal of the Atmospheric Sciences*, *76*(7), 2123-2141. doi: 10.1175/JAS-D-18-0366.1

Hogan, R. J., & Illingworth, A. J. (2000, October). Deriving cloud overlap statistics from radar. *Quarterly Journal of the Royal Meteorological Society*, *126*(569), 2903–2909. doi: 10.1002/qj.49712656914

Hogan, R. J., O'Connor, E. J., & Illingworth, A. J. (2009). Verification of cloud-fraction forecasts. *Quarterly Journal of the Royal Meteorological Society*, *135*(643), 1494-1511. doi: https://doi.org/10.1002/qj.481

Hogan, R. J., Schäfer, S. A. K., Klinger, C., Chiu, J. C., & Mayer, B. (2016, July). Representing 3-D cloud radiation effects in two-stream schemes: 2. Matrix formulation and broadband evaluation. *Journal of Geophysical Research: Atmospheres*, *121*(14), 2016JD024875. doi: 10.1002/2016JD024875

Hogan, R. J., & Shonk, J. K. P. (2013, February). Incorporating the Effects of 3d Radiative Transfer in the Presence of Clouds into Two-Stream Multilayer Radiation Schemes. *Journal of the Atmospheric Sciences*, *70*(2), 708–724. doi: 10.1175/JAS-D-12-041.1

Hourdin, F., Mauritsen, T., Gettelman, A., Golaz, J.-C., Balaji, V., Duan, Q., ... Williamson, D. (2017). The art and science of climate model tuning. *Bulletin of the American Meteorological Society*, *98*(3), 589-602. doi: 10.1175/BAMS-D-15-00135.1

Illingworth, A. J., Hogan, R. J., O'connor, E. J., Bouniol, D., Delanoë, J., Pelon, J., ... others (2007). Cloudnet: Continuous evaluation of cloud profiles in seven operational models using ground-based observations. *Bulletin of the American Meteorological Society*, *88*(6), 883–898.

Jakub, F., & Mayer, B. (2015, September). A three-dimensional parallel radiative transfer model for atmospheric heating rates for use in cloud resolving models—The TenStream solver. *Journal of Quantitative Spectroscopy and Radiative Transfer*, *163*, 63–71. doi: 10.1016/j.jqsrt.2015.05.003

Jakub, F., & Mayer, B. (2017, May). The Role of 1d and 3d Radiative Heating on the Organization of Shallow Cumulus Convection and the Formation of Cloud Streets. *Atmospheric Chemistry and Physics Discussions*, 1–16. doi: 10.5194/acp-2017-415

Joseph, J. H., Wiscombe, W. J., & Weinman, J. A. (1976, December). The Delta-Eddington Approximation for Radiative Flux Transfer. *Journal of the Atmospheric Sciences*, *33*(12), 2452–2459. doi: 10.1175/1520-0469(1976)033⟨2452:TDEAFR⟩2.0.CO;2

Lopes, F. M., Silva, H. G., Salgado, R., Cavaco, A., Canhoto, P., & Collares-Pereira, M. (2018). Short-term forecasts of GHI and DNI for solar energy systems operation: assessment of the ECMWF integrated forecasting system in southern Portugal. *Solar Energy*, *170*, 14-30. doi: https://doi.org/10.1016/j.solener.2018.05.039

Manners, J., Edwards, J. M., Hill, P., & Thelen, J.-C. (2017). *SOCRATES Technical Guide Suite Of Community RAdiative Transfer codes based on Edwards and Slingo* (Tech. Rep.). FitzRoy Rd, Exeter EX1 3PB: Met Office. Retrieved from `http://homepages.see.leeds.ac.uk/~lecsjed/winscpuse/socrates_techguide.pdf`

McKee, T. B., & Cox, S. K. (1974). Scattering of Visible Radiation by Finite Clouds. *Journal of the Atmospheric Sciences*, *31*(7), 1885–1892. doi: 10.1175/1520-0469(1974)031⟨1885:SOVRBF⟩2.0.CO;2

Räisänen, P., & Lindfors, A. V. (2019). On the computation of apparent direct solar radiation. *Journal of the Atmospheric Sciences*, *76*(9), 2761-2780. doi: 10

.1175/JAS-D-19-0030.1

Schäfer, S. A. K., Hogan, R. J., Klinger, C., Chiu, J. C., & Mayer, B. (2016, July). Representing 3-D cloud radiation effects in two-stream schemes: 1. Longwave considerations and effective cloud edge length. *Journal of Geophysical Research: Atmospheres*, *121*(14), 2016JD024876. doi: 10.1002/2016JD024876

Shonk, J. K. P., & Hogan, R. J. (2008, june). Tripleclouds: An Efficient Method for Representing Horizontal Cloud Inhomogeneity in 1d Radiation Schemes by Using Three Regions at Each Height. *Journal of Climate*, *21*(11), 2352–2370. doi: 10.1175/2007JCLI1940.1

Shonk, J. K. P., Hogan, R. J., Edwards, J. M., & Mace, G. G. (2010, July). Effect of improving representation of horizontal and vertical cloud structure on the Earth's global radiation budget. Part I: review and parametrization. *Quarterly Journal of the Royal Meteorological Society*, n/a–n/a. doi: 10.1002/qj.647

Sun, Z., Li, J., He, Y., Li, J., Liu, A., & Zhang, F. (2016). Determination of direct normal irradiance including circumsolar radiation in climate/nwp models. *Quarterly Journal of the Royal Meteorological Society*, *142*(700), 2591-2598. doi: https://doi.org/10.1002/qj.2848

Várnai, T., & Davies, R. (1999). Effects of cloud heterogeneities on shortwave radiation: Comparison of cloud-top variability and internal heterogeneity. *Journal of the Atmospheric Sciences*, *56*(24), 4206–4224.

Villefranque, N., Blanco, S., Couvreux, F., Fournier, R., Gautrais, J., Hogan, R. J., ... Williamson, D. (2021). Process-based climate model development harnessing machine learning: Iii. the representation of cumulus geometry and their 3d radiative effects. *Journal of Advances in Modeling Earth Systems*, *13*(4), e2020MS002423. doi: https://doi.org/10.1029/2020MS002423

Villefranque, N., Williamson, D., Couvreux, F., Hourdin, F., Gautrais, J., Fournier, R., ... Volodina, V. (2020). Process-based climate model development harnessing machine learning: III. The Representation of Cumulus Geometry and their 3D Radiative Effects. *Earth and Space Science Open Archive*, 30. Retrieved from `https://doi.org/10.1002/essoar.10505088.1` (Submitted to JAMES) doi: 10.1002/essoar.10505088.1

Wood, R., Wyant, M., Bretherton, C. S., Rémillard, J., Kollias, P., Fletcher, J., ... Lin, Y. (2015). Clouds, Aerosols, and Precipitation in the Marine Boundary Layer: An Arm Mobile Facility Deployment. *Bulletin of the American Meteorological Society*, *96*(3), 419 - 440. doi: 10.1175/BAMS-D-13-00180.1

Yum, S. S., & Hudson, J. G. (2002). Maritime/continental microphysical contrasts in stratus. *Tellus B: Chemical and Physical Meteorology*, *54*(1), 61-73. doi: 10.3402/tellusb.v54i1.16648